Multiscale Interior Tomography using 1D Generalized Total Variation

Minji Lee, John P. Ward, Michael Unser and Jong Chul Ye*

***Abstract*—We propose a method for accurate and fast reconstruction of the interior of a 2D or 3D tomographic image from its incomplete local Radon transform. Unlike the existing interior tomography work with 2D total variation, the proposed algorithm guarantees exact recovery using a 1D generalized total variation semi-norm for regularization. The restrictions placed on an image by our 1D regularizer are much more relaxed than those imposed by the 2D regularizer in previous works. Furthermore, to further accelerate the algorithm up to a level of clinical use, we propose a multi-resolution reconstruction method by exploiting the Bedrosian theorem for the Hilbert transform. More specifically, as the high frequency part of the image can be quickly recovered using Hilbert transform thanks to the Bedrosian equality, we show that computationally expensive iterative reconstruction can be applied only for the low resolution images in downsampled domain, which significantly reduces the computational burden. We demonstrate the efficacy of the algorithm using circular fan-beam and helical cone-beam data.**

I. Introduction

In x-ray computed tomography (CT), reconstruction of region of interest (ROI) from local projection data has been called for to reduce radiation exposure in imaging specific organs such as heart, or to reduce size of x-ray detector for cost saving. Using the backprojection filtration (BPF) method [1], it was shown that the ROI that cannot cover the whole object can be determined uniquely when the intensity of subregions inside the field of view (FOV) are known *a priori* [2], [3]. However, in general, it is difficult to know the intensity inside the object. Consequently, using the 2D total variation, the authors in [4] showed that unique reconstruction is possible if the images are piecewise constant. In those papers, while the images were assumed to be piecewise polynomial, the regularization term was 2D and fairly complex, which led the authors to focus on piecewise linear images [5]. Furthermore, the iterative procedure to reconstruct the interior images under the regularization is quite complicated, which prohibits its use in clinical environment.

As in those papers, we seek to reconstruct images that are piecewise smooth; i.e., the domain where the image is defined can be decomposed into a finite number of subdomains such that the image is a smooth function on each piece. However, our approach generalizes the ideas developed in [5] with a simplified 1D formulation, and as a result, we are able to perfectly reconstruct new classes of functions. In particular, we can reconstruct any image that is a generalized L-spline along a collection of lines passing through the region of interest. Here L is a differential operator that can be more general than an n-th order derivative. For example, we can reconstruct images whose 1D restrictions are non-polynomial exponential B-splines, and which are not covered by the previous works.

To further accelerate the algorithm up to a level of clinical use, we propose a multi-scale reconstruction method that separately reconstructs low frequency part and high frequency part of the 1D signal at different resolution. More specifically, thank to the Bedrosian equality for the Hilbert transform, even for the truncated Hilbert transform, we can show that high frequency part of the signal can be recovered accurately using one step Hilbert transform. Therefore, the computationally expensive iterative reconstruction can be performed only to reconstruct the low frequency part of the signal after down-sampling, which allows its fast implementation. We verify the efficacy of the algorithm using 2D fan-beam and 3D cone-beam reconstruction with realistic acquisition parameters.

M. Lee and J. C. Ye are with Bio Imaging & Signal Processing Lab, Department of Bio & Brain Engineering, KAIST, Korea. J. P. Ward and M. Unser are with Bioimaging Group, EPFL, Switzerland.

II. Mathematical Backgrounds

A. Differentiated Backprojection and Hilbert Transform

In helical cone-beam CT, the scanning trajectory is expressed as

$$\vec{r}_0(\lambda) = \left(R\cos(\lambda), R\sin(\lambda), \frac{h}{2\pi}\lambda \right)^T , \qquad (1)$$

where λ is the rotation angle of x-ray source, R the distance from the source to rotation axis, and h the pitch of helical trajectory. If $h = 0$, the acquisition geometry is reduced to a 2D fan-beam geometry. From helical cone-beam scanning, we can get the cone-beam projection data of a 3D object function $f(\vec{r})$, and it can be expressed as

$$P(\vec{r}_0, \hat{\beta}) = \int_0^\infty ds \; f(\vec{r}_0 + s\hat{\beta}), \quad \hat{\beta} \in S^2 \qquad (2)$$

with the unit vector $\hat{\beta}$ of projection direction from a x-ray source location at $\vec{r}_0$. From this projection data, the differentiated backprojection (DBP) at the 3D point $\vec{r}$ can be computed by [1]

$$g(\vec{r}) = \frac{-1}{2\pi} \int_{\lambda_1}^{\lambda_2} \frac{d\lambda}{|\vec{r} - \vec{r}_0(\lambda)|} \frac{\partial}{\partial q} P\left(\vec{r}_0(q), \hat{\beta}(\lambda, \vec{r})\right)\Big|_{q=\lambda} . \qquad (3)$$

In this equation, $\frac{\partial}{\partial q} P\left(\vec{r}_0(q), \hat{\beta}(\lambda, \vec{r})\right)\Big|_{q=\lambda}$ means differentiation of projection with respect to the source trajectory, and $\int_{\lambda_1}^{\lambda_2} \frac{d\lambda}{|\vec{r} - \vec{r}_0(\lambda)|}$ refers the backprojection with cone-beam weighing. Here, λ_1 and λ_2 are determined by a PI line through $\vec{r}$. This PI line is unique for any point inside the helix, so

there must be unique λ_1 and λ_2 for $\vec{r}$. Now, with a slight abuse of notation, if we define DBP data and attenuation image restricted on the PI line as

$$g(x) := g\left(\vec{r}_0(\lambda_1) + x(\vec{r}_0(\lambda_2) - \vec{r}_0(\lambda_1))\right) \quad (4)$$
$$f(x) := f\left(\vec{r}_0(\lambda_1) + x(\vec{r}_0(\lambda_2) - \vec{r}_0(\lambda_1))\right) . \quad (5)$$

Then, we have the following 1D Hilbert transform relationship

$$g(x) = \frac{1}{\pi}\text{P.V.}\int_{-\infty}^{\infty}\frac{dx'}{x-x'}f(x') = \mathcal{H}f(x) \quad (6)$$

where P.V. denotes the Cauchy principal value. For the case of 2D fan-beam geometry, the PI line is not unique and we can choose infinitely many PI lines that pass through $\vec{r}$. Among these, we use a set of PI lines that are parallel to each other to simplify the implementation.

B. Interior Tomography Formulation

If the DBP data $g(x)$ is available for all x, the reconstruction of $f(x)$ can be simply done by performing inverse Hilbert transform $\mathcal{H}^{-1}$, which is equal to $-\mathcal{H}$. However, in the case of interior tomography problem, the detector is truncated; so, the DBP data is only available within $x_1(e_1, e_2)$. The main problem of such truncated Hilbert transform is the existence of the null space. More specifically, there exists non-zero $\nu(x)$ such that

$$\mathcal{H}\nu(x) = 0, \quad x \in (e_1, e_2) . \quad (7)$$

Indeed, $\nu(x)$ can be expressed using an appropriate DBP data $h(x)$ outside of the ROI:

$$\nu(x) = -\frac{1}{\pi}\int_{\mathbb{R}\setminus(e_1,e_2)}\frac{dx'}{x-x'}h(x') . \quad (8)$$

Then, a required interior tomography formulation is to find an appropriate regularization term that suppresses the signal belonging to the null space of the truncated Hilbert transform. Note that $\nu(x)$ in (8) is differentiable in any order due to the removal of the origin in the integrand.

III. Main Contributions

A. Exact Recovery under Generalized TV Penalty

To generalize the TV to meet the goal, we consider a regularization with respect to a Fourier multiplier operator L that is defined on $L_2(\mathbb{R})$ and satisfies two conditions. First, for any interval $E = (e_1, e_2) \subset \mathbb{R}$, we require L to map $C_c^\infty(E)$ to $C_c(E)$. Second, the null space of L, denoted as $\mathcal{N}_\text{L}$, should consist of entire functions. An example of such an operator is a constant coefficient differential operator

$$\text{L} := a_K\text{D}^K + a_{K-1}\text{D}^{K-1} + \ldots + a_1\text{D} + a_0 \quad (9)$$

where $K \geq 1$, D denotes the distributional derivative on $\mathbb{R}$, and each a_k is a real number. In this example, the finite-dimensional null space consists of linear combinations of exponential functions multiplied by polynomials. For an operator L and an interval $E \subset \mathbb{R}$, we formally define the *generalized total variation semi-norm*

$$\|f\|_{TV(\text{L};E)} := \|\text{L}f\|_{L_1(E)} \quad (10)$$

which is valid when $\text{L}f \in L_1(E)$. In order to ensure that this semi-norm is valid for a larger class of functions, we use the dual formulation

$$\|f\|_{TV(\text{L};E)} := \sup_{h\in C_h}\int_E f(x)\text{L}^*h(x)dx \quad (11)$$

where $C_h = \{h \in C_c^\infty(E), \|h\|_{L_\infty} \leq 1\}$. As in [4], our results are based on the fact that $\nu(x)$ in (8) is infinitely smooth in E. Suppose, furthermore, the signal $f(x)$ to be reconstructed is a generalized L-spline, where L is a finite-order operator. It is this disparity between the infinitely smooth $\nu(x)$ and the finitely smooth $f(x)$ that allows us to have perfect reconstruction.

Theorem 1. *Let $f_0(x)$ be a generalized* L*-spline such that*

$$\text{L}f_0(x) = \sum_{n=1}^{N} a_n\delta(x - x_n) \quad (12)$$

on E. Then, the following minimization problem

$$\arg\min_f \|f\|_{TV(\text{L};E)} \quad \textit{subject to } \mathcal{H}f_0(x) = \mathcal{H}f(x), \quad x \in E$$

has the unique solution equal to $f_0(x)$.

B. Multi-Resolution Decomposition Using Bedrosian Equality

Unlike the previous works [5], our regularization is based on 1D TV semi-norm. Therefore, the optimization problem is much less complex. In addition, we now propose a multi-scale decomposition method that further reduces the computational complexity.

1) Low frequency reconstruction: To reconstruct $f(x)$ from its truncated Hilbert transform, we split it into low-pass and high-pass components. This is accomplished by convolving with a function ϕ whose Fourier transform Φ satisfies:

- For some $\omega_0 > 0$, $\Phi(\omega) = 1$ when $|\omega| < \omega_0$ and $\Phi(\omega)$ has fast decay for $|\omega| > \omega_0$;
- Φ is even, smooth, and decreasing for $|\omega| > \omega_0$

In this paper, we use a spline for ϕ. Then, the low-pass component $f_L(x)$ is given by convolving $a_f^{-1}\phi(a_f)$ with $f(x)$, for some dilation factor $a_f > 0$. This can be easily implemented using spline wavelet transform and taking the lowest band signal. Furthermore, the low-pass component $f_L(x)$ can be recovered from the corresponding low-pass component of the DBP data $g(x)$ since the Hilbert transform preserves the bandwidth as observed in

$$G(\omega) = \mathcal{F}\{\mathcal{H}f\}(\omega) = -i\,\text{sgn}(\omega)F(\omega). \quad (13)$$

Thanks to (13), we can reconstruct the $f_L(x)$ from the down sampled DBP data $g_L(x)$. For the recovery of the resulting low-pass band $f_L(x)$, we make the following assumption.

Assumption 1. *f_L is well modeled as an* L*-spline for some Fourier multiplier operator* L.

Under this assumption, f_L is reconstructed using the iterative algorithm with TV semi-norm regularization. The implementation of the iterative step will be explained in detail later.

2) High frequency reconstruction: After reconstructing $f_L(x)$, the high-pass component $f_H(x)$ is the complement. Note in particular that the Fourier transform of f_H is identically zero in a neighborhood of the origin. This allows us to compute f_H using Bedrosian's theorem for the Hilbert transform.

Theorem 2 (Bedrosian)**.** *Let $f, g \in L_2(\mathbb{R})$. Suppose that the Fourier transform of f, denoted by $F(\omega)$, vanishes for $|\omega| > \omega_0$, with $\omega_0 > 0$, and the Fourier transform of g, denoted by $G(\omega)$, vanishes for $|\omega| < \omega_0$; then*

$$\mathcal{H}\{f(x)g(x)\} = f(x)\mathcal{H}g(x) \ . \tag{14}$$

Since we only have exact data for $\mathcal{H}f(x)$ on a restricted interval $E = (e_1, e_2)$, we apply a band-limited finite length window $w(x)$ before computing the inverse Hilbert transform. Bedrosian's theorem implies that

$$w(x)g_H(x) = w(x)\mathcal{H}f_H(x) = \mathcal{H}\{w(x)f_H(x)\} \tag{15}$$

as long as the support of $W(w)$ is contained in a neighborhood of the origin that is disjoint from the support of $F_H(w)$. Here, we use the characteristic function of the interval $E = (e_1, e_2)$. Solving for f_H in (15), we get

$$f_H(x) = \frac{-\mathcal{H}\{w(x)g_H(x)\}}{w(x)}, \quad x \in E \ . \tag{16}$$

IV. Implementation

A. Low Frequency Signal Reconstruction

To recover the low frequency signal, we first take downsampling of the original DBP by wavelet decomposition and taking the lowest frequency band (see Fig. 1). From the downsampled DBP signal, the low frequency part of signal is reconstructed using projection onto convex sets (POCS) algorithm, and the reconstructed signal is then upsampled to the original resolution signals. This procedure takes much less time than iterative reconstruction of the original full-resolution DBP signal. For POCS implementation, the following five convex constraint sets are used:

$C_1 = \{f(x) \in L^2(\mathbb{R}) : f(x) = 0, x \notin (b_1, b_2)\}$
$C_2 = \{f(x) \in L^2(\mathbb{R}) : \mathcal{H}f(x) = g(x), x \in (e_1, e_2)\}$
$C_3 = \{f(x) \in L^2(\mathbb{R}) : \|f\|_{TV(\mathrm{L};E)} \leq \tau\}$
$C_4 = \{f(x) \in L^2(\mathbb{R}) : \int_{b_1}^{b_2} dx f(x) = P(\vec{r}_0(\lambda_1), \hat{\beta}(\lambda_1, \vec{r}))\}$
$C_5 = \{f(x) \in L^2(\mathbb{R}) : f(x) \geq 0, \forall x\}$,

Here, (b_1, b_2) denotes the approximate object boundary. The projection to each constraint is quite straightforward except for the projection on C_3, the generalized TV norm constraint. It turns out that the projection on C_3 from a point f_0 can be implemented as the following denoising step.

$$\hat{f} = \arg\min_f \left\{\|f - f_0\|_2^2 + 2\lambda\|f\|_{TV(\mathrm{L};E)}\right\} \tag{17}$$

for an appropriate Lagrangian parameter. Using the definition of the generalized TV semi-norm, the optimization problem is given by

$$\sup_{h \in C_h} \min_f \left\{\|f - f_0\|_2^2 + 2\lambda\langle f, \mathrm{L}^* h\rangle\right\} \ , \tag{18}$$

whose optimal solution of the inner minimization is given by $\hat{f} = f_0 - \lambda \mathrm{L}^* h$. So, (18) can be reformulated with respect to the dual variable:

$$\min_{h \in C_h} \left\{\lambda^2 \|\mathrm{L}^* h\|_{L_2(E)}^2 - 2\lambda\langle f_0, \mathrm{L}^* h\rangle\right\} \ . \tag{19}$$

Then, the optimal solution $\hat{h}$ can be obtained by gradient projection method

$$h_k = P_{C_h}\left(h_{k-1} - 2t_k\lambda \mathrm{L}\left(\lambda \mathrm{L}^* h_{k-1} - f_0\right)\right) \tag{20}$$

when t_k denotes the k-th step size, P_{C_h} denotes the projection on the convex set C_h, and $2\lambda \mathrm{L}(\lambda \mathrm{L}^* h - f_0)$ is the gradient of the cost function in (19). For super-linear convergence rate, we implement the algorithm based on Nestrov method.

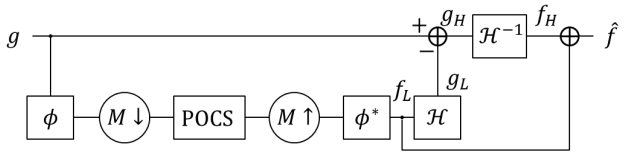

Fig. 1. Multi-resolution reconstruction flowchart.

B. High Frequency Signal Reconstruction

After low frequency reconstruction, the reconstructed low frequency signal is upsampled using wavelet reconstruction. The upsampled low resolution image is then transformed using Hilbert transform to extract the high frequency residual DBP signals. Then, the resulting high frequency residual signal is applied to an inverse Hilbert transform to obtain high frequency signal. Finally by adding the reconstructions of low and high frequency, we can get the interior tomography with the original resolution (see Fig. 1).

V. Numerical Results

A. Circular Fan-Beam CT

The first reconstruction result was obtained with circular fan-beam projection. The 2D phantom is 512×512 size with 1×1 mm^2 size pixel. The number of detector array is 400 with 1 mm pitch, and the number of views is 1200. The distance from source to rotation axis is 800 mm, and the distance from source to detector is 1400 mm. The radius of FOV is about 113 mm, so for each PI line, the truncation rate (length of support divided by length of FOV) is from 0 to 0.95. In Fig. 2, the first image in (a) is the original ground truth. Fig. 2(b)(c) show the low and high frequency reconstruction images respectively, and the final reconstruction is shown in Fig. 2(d), which is nearly identical to the original signal.

B. Helical Cone-Beam CT

The second simulation is 3D cone-beam CT with helical trajectory. The resolution of the phantom is 512×512×512 voxels with voxel size $1\times1\times1$ mm^3. The distances from source to rotation axis and from source to detector are same with the circular fan-beam simulation. The detector resolution is 450×109 pixels with pitch of 1×1 mm^2, so the radius of

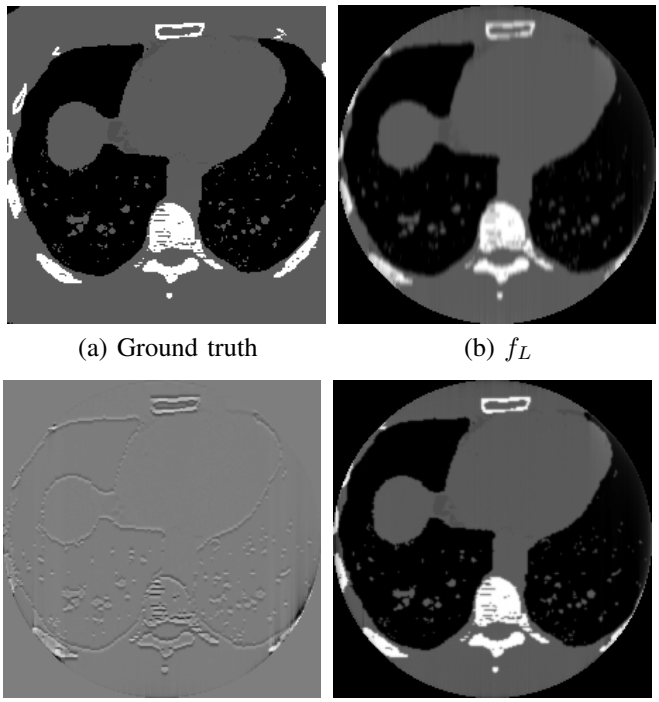

(a) Ground truth (b) f_L

(c) f_H (d) $f_L + f_H$

Fig. 2. 2D fan-beam reconstruction: (a) ground truth, (b) low frequency signal reconstruction, (c) high frequency signal reconstruction, and (d) the final reconstruction result.

FOV is about 127 mm. For helical scanning trajectory, the number of rotations is 3, the helical pitch h is 100 mm, and the number of views is 1200 per rotation. First, the object was reconstructed in PI line space, and then by regridding process, the final reconstruction of about 250 slices was obtained.

Fig. 3 is the reconstruction result in FOV for the helical cone-beam CT. Even for helical cone-beam CT, the original 3D problem can be converted into many 1D problems on the PI line, so what we need to do is repeat the 1D reconstruction processes for all PI lines. In the first column, transection, coronal, and sagittal planes are shown, and for each row, the line profile whose location is indicated by white line in the plane image was plotted. The total computational time was less than 14 minutes, which corresponds to about 3 seconds for each slice.

VI. Conclusions

Using the differentiated back projection, an interior tomography problem in 2D or 3D can be converted to a 1D truncated Hilbert transform problem. Due to the existence of the null space in the truncated Hilbert transform, appropriate regularization is necessary. To overcome the complexity and restriction of the existing 2D-TV regularization approach, this paper proved that 1D generalized TV semi-norm penalty is more relaxed but still sufficient to guarantee the perfect recovery. Moreover, by exploring the Bedrosian theorem, we demonstrated that the computational expensive iterative reconstruction can be performed at very coarse resolution, which significantly reduces the computational complexity. The simulation result shows the proposed algorithm can produce high quality reconstruction for both 2D and 3D geometries, and its computational time can be significantly reduced down to practical level even for helical cone-beam CT.

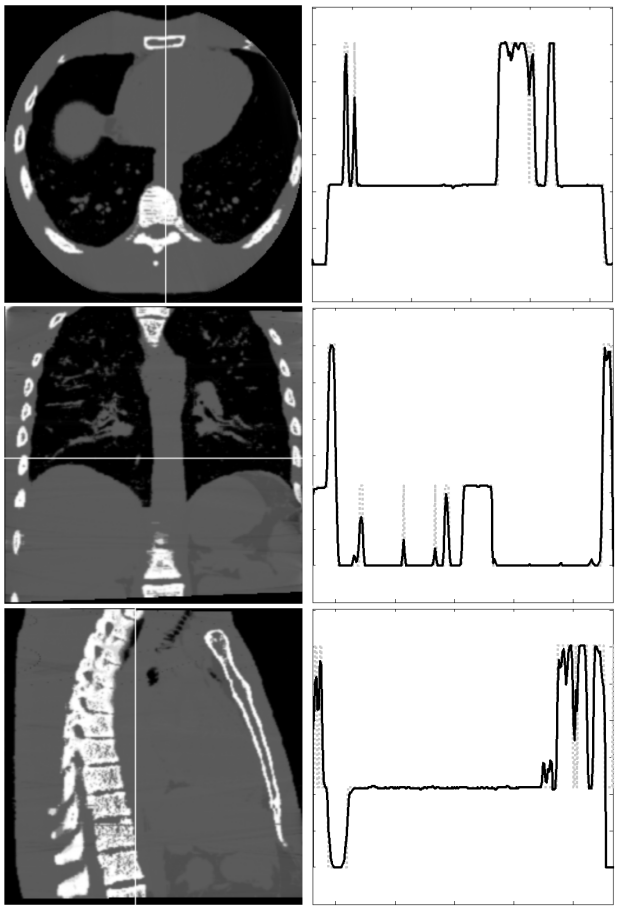

Fig. 3. Reconstruction images and line profiles with 3D inner organ phantom and helical cone-beam scanning

Acknowledgment

MJL and JCY were supported by the National Research Foundation of Korea (NRF) grant No.2009-6081089, and Samsung Electronics. The research leading to these results by JPW and MU has received funding from the European Research Council under the European Union's Seventh Framework Programme (FP7/2007-2013) / ERC grant agreement n 267439.

References

[1] Yu Zou and Xiaochuan Pan, "Image reconstruction on pi-lines by use of filtered backprojection in helical cone-beam ct," *Physics in medicine and biology*, vol. 49, no. 12, pp. 2717, 2004.

[2] M. Defrise, F. Noo, R. Clackdoyle, and H. Kudo, "Truncated Hilbert transform and image reconstruction from limited tomographic data," *Inverse Problems*, vol. 22, no. 3, pp. 1037, 2006.

[3] M. Courdurier, F. Noo, M. Defrise, and H. Kudo, "Solving the interior problem of computed tomography using *a priori* knowledge," *Inverse problems*, vol. 24, no. 6, pp. 065001, 2008.

[4] H. Yu and G. Wang, "Compressed sensing based interior tomography," *Physics in medicine and biology*, vol. 54, no. 9, pp. 2791, 2009.

[5] Jiansheng Yang, Hengyong Yu, Ming Jiang, and Ge Wang, "High-order total variation minimization for interior tomography," *Inverse problems*, vol. 26, no. 3, pp. 035013, 2010.